Fourier decomposition of the transverse field for analyzing optical waveguides using beam propagation method

SANJEEV KUMAR RAGHUWANSHI*, SRINIVAS TALABATTULA AND A. SELVARAJAN
Applied Photonics Laboratory, Department of Electrical Communication Engineering, Indian Institute of Science, Bangalore 560 012, India.
email: sanjeevkr@ece.iisc.ernet.in, Phone: +91-80-2293 2852, Fax: +91-80-2360 0563.

Abstract

Analytical solutions of the wave equation exist only for a few waveguide structures. Direct numeric solution of the wave equation is possible for many structures, although this usually involves iteration to find the approximate eigenvalue. This paper studies the modes of structures, otherwise not amenable to analytic or approximate solution, by integrating Fourier decomposition of the transverse field with the Beam propagation method (BPM). Numerical simulations of special structures such as waveguides with bends or reflective mirrors, split Y-couplers and coupled adjacent waveguides have been carried out. We also examine the operation of a coupled waveguide and apply its theory to calculate its performance to compare it with simulation.

Keywords: Beam propagation method, Fast Fourier transform, waveguide structures, beam diffraction, waveguide coupler.

1. Introduction

A Y-coupler, shown in Fig. 1(a), is a simple device that connects one waveguide to two waveguides [1–4]. Since the mode dynamically changes as it enters the structure, it is difficult to calculate the loss the mode encounters and the optimum angle to split the waveguide. Numerical simulation methods allow us to determine these answers.

BPM is numerical simulation of the field in a guide, in contrast to the numerical solution of the exact wave equation [5–8]. Simulations are often the only way to determine the mode profile in an unusual waveguide and to map out the behavior of a mode as the index profile changes along *z*. This latter effect is very common in practical devices, such as waveguide tapers or waveguide perturbed by a second nearby waveguide. BPM works by decomposing a spatial mode into a superposition of plane waves, each travelling in a slightly different direction. After advancing each wave a certain distance through dielectric structure of interest, the plane waves are added back together to reconstruct the spatial mode. This process requires the use of Fourier transforms to convert from the spatial mode to the superposition of plane waves and back again. BPM is a quite established numerical method, but is not a widely used Fourier decomposition technique. This paper presents a scalar BPM with

---

*Author for correspondence.
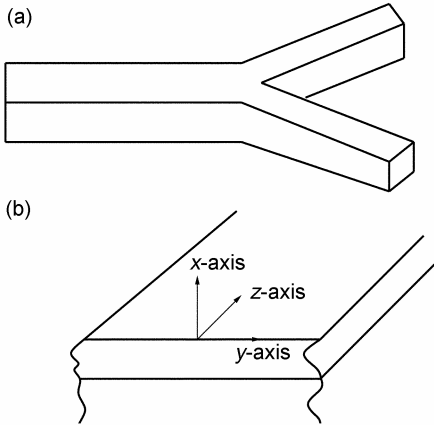
(a)

(b)

x-axis

z-axis

y-axis

FIG. 1. (a) A Y-coupler is a simple device that couples one waveguide to two waveguides. (b) An infinite slab dielectric waveguide. The wave is presumed to travel in *z*-direction.

Fourier decomposition of the transverse field for analyzing optical waveguides. This paper reviews the current literature and provides an introduction to vector beam propagation methods and other advanced techniques.

2. Superposition of waves and fast Fourier transform

Consider the planar slab waveguide, where the index profile varies only in the *x*-direction (Fig. 1(b)). Due to symmetry, the spatial field is functionally independent of *y*-direction. A guided field in such a source-free dielectric structure must be a solution to the wave equation

$$\nabla^2 \psi + k_0^2 n^2(x)\, \psi = 0, \tag{1}$$

where $\psi(x, z, t)$ is a vector function describing the amplitude, polarization and direction of field propagation. If the waveguide consists of isotropic regions, i.e. the index does not have a gradient profile, the spatial solution to the scalar wave equation in each region of space is simply a plane wave,

$$\psi_i(x, z, t) = A_i e^{-j(k_x x + k_z z)} e^{j\omega t} + c.c., \tag{2}$$

where A_i is the amplitude in the region i and the k vector (described in terms of its components) depends on the frequency of the wave and the local index of refraction and can be real or imaginary. Boundary conditions connect the solutions at the interfaces separating different regions. Plane waves are the natural solution to wave equation. Since the wave eqn (1) is linear, any linear superposition of solutions will also constitute a valid solution. This important fact forms the foundation of the technique used to numerically analyze the fields in a waveguide. We used a superposition of plane waves, each with identical angular frequency ω but different values of k to describe the general mode of a waveguide. The plane waves form a basis set for mode description. Describing a spatial function $\psi(x)$, in terms of a superposition of plane waves e^{jkx},

$$\psi(x) = \sum A_i e^{jk_i x}, \tag{3}$$

should remind us of the Fourier transform. To illustrate, consider an one-dimensional electric field distribution with a Gaussian distribution.

$$\psi(x) = E_0 e^{-x^2/x_0^2}. \tag{4}$$

The Gaussian profile describes the lowest order mode in a parabolic index profile waveguide. Also, we are familiar that the modes of laser beams in free space would recognize this profile as the fundamental TEM_{00} mode of a Hermite–Gaussian beam. To describe this transverse spatial mode in terms of a superposition of plane waves e^{jkx}, we employ the Fourier transform pair,

$$\psi(x) = \frac{1}{2\pi} \int_{-\infty}^{\infty} A(k_x) e^{jk_x x} dk_x, \tag{5}$$

$$A(k_x) = \int_{-\infty}^{\infty} \psi(x) e^{-jk_x x} dx, \tag{6}$$

where k_x is the x component of the wavevector k. The transform of $\psi(x)$ yields $A(k_x)$, which is a complex number that contains information about the amplitude and phase of each plane wave component. Equation (6) can be readily evaluated to give amplitudes for Gaussian input pulse eqn (4)

$$A(k_x) = \frac{1}{\sqrt{\pi x_0^2}} e^{-\pi^2 x_0^2 k_x^2}. \tag{7}$$

Recall that the magnitude of k is identical for all components in a mode, only k_x and k_z components vary. Simple trigonometry provides the value of the z-component of the wave vector $k_z = \sqrt{k^2 - k_x^2}$. The largest k_z-vector has $k_x = 0$, corresponding to a plane wave travelling along the z-axis. As the k_x component increases, the amplitude of the plane wave decrease (eqn (7)). The Fourier transform pair in eqns (5), and (6) allows us to readily convert a wave described in the spatial domain $\psi(x)$ to a wave described in phase space domain $\psi(k)$. In the BPM method, propagation effects are calculated using the phase space representation and phase shifts caused by the waveguide structure and are introduced using the spatial representation of a mode. We use both these transforms to alternately convert a spatial field into a superposition of plane waves and back again. To take advantage of numerical computers for calculating FFT, we use discrete Fourier transforms based on what is generically called fast Fourier transform. FFT algorithms are widely available in literature [9] and are common features in engineering and mathematical numerical software packages for work stations and personal computers. Application of FFT to optical propagation problems is discussed in Buckman [10]. FFT is closer in operation to a Fourier series than to a Fourier transform. Recall that a Fourier series is used to describe a periodic function in terms of a discrete set of sinusoidal basis states. FFT describes a distribution in terms of a large but finite number of discrete sinusoidal waves with appropriate amplitude. The effect of discrete sampling can lead to the creation of aliases of the waveform. This fact introduces a complication in the BPM calculation. To find the FFT of a spatial profile, the profile must first be represented as a numeric array. The sampling resolution must be fine enough to
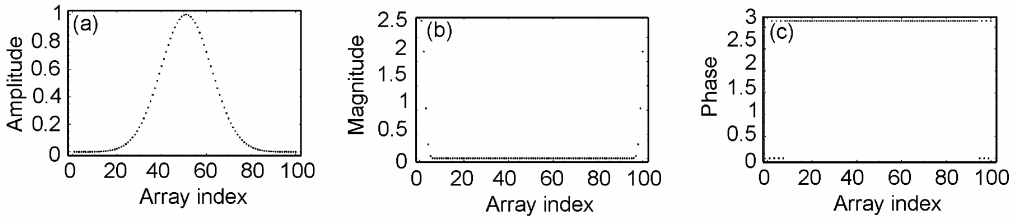
FIG. 2. (a) The sampled profile of a Gaussian mode, (b) The FFT of the Gaussian profile is plotted as a function of the array index, and (c) The phase (radians) of the DFT of the Gaussian wave is shown in Fig. 2(a).

resolve all spatial features of the amplitude profile, yet at the same time be sparse enough to allow reasonable processing speed on a computer. In the calculations that follow, an array with 100 points proved adequate to see the desired behavior. Let's begin a demonstration of the BPM using Gaussian mode profile. Since the evanescent amplitudes follow an exponential decay, they never truly go to zero. Theoretically there will be some error introduced when we restrict the spatial domain to something less than infinity. If we extend the sampling domain out to three or four characteristic decay lengths, we can usually get satisfactory results. In this example, we sampled the profile in Fig. 2(a) at 100 equally spaced discrete points ranging from $x = -25$ μm to $x = 24.5$ μm. Since the profile is assumed to be periodic in an FFT (this means that the algorithm assumes that if it looked at points 101 to 200, it would find another Gaussian wave of the same shape and amplitude centered near point 150), the data point at $x = -25$ μm is same as at $x = 25$ μm, so it is important to not include this point twice in the array. That is why the domain is selected as shown in Fig. 2(a), which shows the resulting array. The abscissa is the array index, not the position.

Having established an array, we have computed the DFT of the spatial profile in order to determine the superposition of plane waves that comprise the mode. The FFT of the N point array is itself an N point array, found by approximating the integral in eqn (4) with a discrete summation. The N complex numbers which describe the spatial amplitude are converted into N complex numbers which correspond to the amplitude and the phase of each plane wave component with $k_x = \frac{2\pi(s-1)}{H}$, where H is the spatial size of the sample and s runs from 0 to N. The magnitude of these amplitudes for the Gaussian profile is plotted in Fig. 2(b), where the abscissa is the s index. There are in fact 100 points in the FFT, exactly the same number as is in the amplitude array. The appearance of the FFT is a little strange at first glance. Instead of producing a smooth peak in k space, we find a distribution with non-negligible values near $s \approx 0$ and $s \approx 100$, but very little magnitude at mid-range values. The strange structure of the FFT arises because the Fourier transform is calculated on a discrete array of samples from the actual waveform. The value of the FFT at $s = 1$ corresponds to the average value of the spatial profile, the $k_x = 0$ term of the expansion. The next few terms describe the $k_x = \frac{2\pi(s-1)}{H}$ components of the transverse k vector, where H is the domain of the spatial wave. Each additional point corresponds to the next higher transverse component. In this example, we choose $H = 50$ μm. From the FFT, it is clear that there are not many higher-order transverse components needed to describe this mode. Now turning to terms near $s = 100$, the periodic sampling of the mode profile, those with $s = 99$ correspond to $s = -1$ or $k_x = -\frac{2\pi}{H}$. Similarly, $s = 98$ corresponds to $s = -2$ and so forth. Physically, these

correspond to plane waves traveling with slight downward inclination, while the plane waves with values such as $s = 2$ correspond to plane wave travelling with a slightly positive inclination. Figure 2(c) shows the plot of the phase of the FFT of the Gaussian beam. Notice that in the region where there is significant amplitude for FFT, the phase alternates between 0 and π. The phase tells us what the wavefront curvature of the beam is. In this case the field is everywhere real, indicating that it represents a plane wave.

3. Beam diffraction

A wavefront is a locus of points where the phase is constant. Complex numbers convey phase information in a wave. Since the equation which describes the Gaussian mode, eqn (4), is purely real, the phase is constant as a function of position vector, so the mode has a planar wavefront. If the phasefront of the mode had some curvature, the phase would change with distance from the axis and the proper description of this would involve using complex numbers. In general, the array used to describe the spatial waves and the Fourier amplitudes would be complex. By describing a real beam as a superposition of plane waves, we can develop an accurate method for simulating beam propagation which includes effects such as diffraction. In this section, we show how the previous analysis of plane wave superposition can numerically determine the beam diffraction of a propagating field. This step incidentally is the first step in understanding the BPM. Let's propagate a wave a distance L in the z direction using the plane wave method. We first decompose spatial profile into a superposition of plane waves and then advance each plane wave component forward to the plane $z = L$. Later, we superimpose these plane waves back together to form the new spatial mode. Since each plane wave travels in a different direction, each would accumulate a different amount of phase due to the path length difference incurred travelling to the plane at $z = L$. Figure 3(a) shows a geometric argument for the phase shift. Every plane wave component of the expansion has a wavevector with magnitude k, that travels in a unique direction. A component travelling at an angle $\theta (\theta = \sin^{-1}(\frac{kx}{|k|}))$ with respect to z-axis will travel a slightly longer distance, $L' = \frac{L}{\cos\theta}$, to reach the plane at $Z = L$, than a wave travelling parallel to z-axis. Using the small-angle approximation for θ and the fact that in FFT, $k_x = \frac{(s-1)2\pi}{H}$ and $|k| = \frac{2\pi}{\lambda}$, the phase accumulated by each ray is given by,

$$\phi_s = \frac{kL}{\cos\theta} = kL\left[1 + \frac{k_x^2}{2n^2k_0^2}\right] = kL\left[1 + \frac{\lambda^2}{2H^2}(s-1)^2\right], \tag{8}$$

where H is the size of the spatial domain of the amplitude profile. The term s refers to the index of the $(s-1)^{th}$ spatial frequency component of the plane wave superposition. For example, $s = 1$ corresponds to $k_x = 0$ of the Fourier expansion. Each Fourier component will accumulate a different amount of phase after traveling along the z-axis because they each of them traverse a slightly different path length. We are now ready to propagate the optical mode distance through space. We do this in two steps. First, we must determine the plane wave superposition that comprises the initial spatial field. This has been described above using the FFT of the spatial function $E(x)$. Next we let each component of the wave propagate up to the plane at $z = L$. Since nothing alters the magnitude of the individual plane waves as they propagate, the amplitude of each component remains the same. However, since they accumulate different amounts of phase based on the difference in path length, we
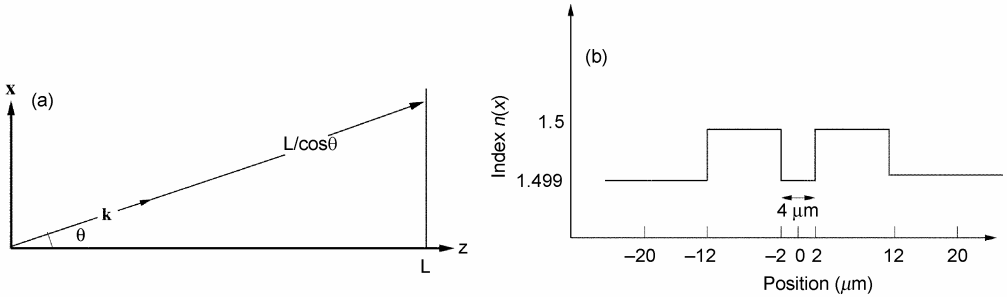
FIG. 3. (a) Geometrical picture of path a plane must follow to move the distance L along the z-axis. (b) Index profile of two slab waveguides separated by only 4 μm.

have to add a proper amount of phase to each component. Consider the Gaussian mode shown in Fig. 2(a). We assume that it represents a TEM_{00} laser beam with wavelength 0.8 μm and furthermore we assume that the profile represents the beam at focus, so the wavefront is planar. We use the BPM to calculate how the beam spreads and develops wavefront curvature as it travels through free space. Since diffraction theory has well-established analytic expressions for describing Gaussian beam diffraction, we can use these to confirm the operation of the BPM technique. We start with an expression for the beam at $z = 0$. The beam is a simple Gaussian profile with characteristic length of 8 μm,

$$E(x, 0) = A.e^{-x^2/8^2}, \tag{9}$$

where all dimensions are in μm and A is an arbitrary amplitude which we would have set to unit. Notice that the wave is everywhere real, showing that the field is a plane wave at $z = 0$. We must determine the FFT of this mode by first creating an array of equally spaced samples of the amplitude. Various situations are discussed in Fig. 4. Figure 4(f) shows the calculated amplitude at $z = 0$, $z = 500$ and $z = 1000$ μm. The amplitude decreases as the width increases, conserving total power. The amplitude ripple apparent in Fig. 4(f) for the profile at $z = 1000$ μm is an artifact of the FFT and is not a true representation of the profile. Due to the periodic nature of the FFT, high spatial frequency components that travel out of the field on to the right side of the spatial domain reappear on the left-hand side and vice versa. One way to avoid this is to increase the domain size H, but this just delays the onset of the problem. A second method is to apodize the domain, effectively adding an attenuation near the edge of the spatial domain. We have introduced the latter method to BPM to dissipate these waves before they reappear on the other side.

4. Beam propagation method and numerical example

We can apply the principles of beam propagation to guided wave problem. BPM is motivated by two physical properties of electromagnetic waves. First, as we have just seen, a wave traveling through any region of space will diffract. Second, the phase shift accumulated by the wave as it propagates in the forward direction depends on the local index of refraction. In an inhomogeneous medium, a wave would accumulate phase depending on the distance travelled and on the local index of refraction. The effects of propagation and local index act continuously on the phase as the wave travels but we have numerically simulated
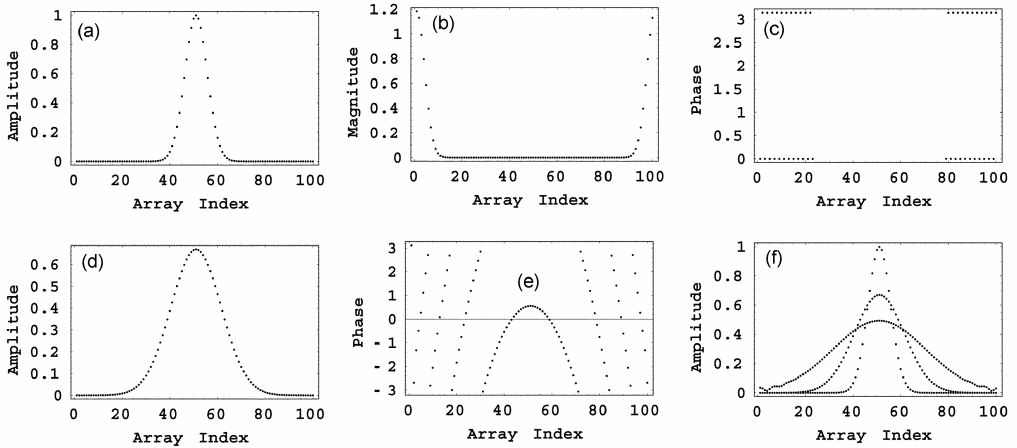
FIG. 4. (a) The waveform described in eqn (9) is sampled at 100 discrete points. (b) The magnitude of the FFT of array is shown as a function of the array index. In this case, the array index corresponds to transverse momentum of $k_x = \frac{2\pi(s-1)}{120}$ μm^{-1}. (c) The phases of the Fourier components of the DFT of the spatial mode are shown as a function of array index. All phases are either 0 or 180°, implying that the wave has no curvature and is therefore a plane wave. (d) The amplitude of the Gaussian field after travelling 500 μm. (e) The phase of the mode after travelling 500 μm has picked up considerable curvature. The phase shift increases quadratically with distance from the axis; however, the amplitude rapidly decreases, so the phase information is only significant near the axis. (f) The amplitude profile of the mode at $z = 0$ μm (ampl. = 1), $z = 500$ μm (ampl. = 0.6) and $z = 1000$ μm (ampl. = 0.4).

this process in a series of small steps. The local index is modeled as a sequence of lenses separated by short regions of homogeneous space index $\bar{n}$, which is the average of the refractive index that the beam travels through between adjacent lenses. The beam propagation method uses a split step process. In the first step, the transverse electric field at position z, $\psi(x, y, z)$ decomposes into a superposition of plane waves $\psi_i(k) = A_i e^{jk_i \cdot r}$ via fast Fourier transform and propagates a distance Δz as if it were travelling through an index $\bar{n}$. We have already discussed how to perform this step. Following the propagation step, an inverse FFT converts the superposition of plane waves back into a spatial field. The second step adds the phase correction needed to account for the spatial structure of the index profile. As the wave propagates from z to $z + \Delta z$, different part of the phase front will experience different amounts of phase shift depending on the local index of refraction $n(x, y, z)$. We adjust the step size so that the accumulated phase corrections are small following each step. Typical step sizes are of the order of a μm. The spatial phase correction is added to the spatial wave. The resulting field is a reasonable representation of the actual field distribution at location $z + \Delta z$. The new field serves as the source field for the next propagation step. BPM repeats this two-step process until the wave has traveled the desired distance. Introducing the lens step is surprisingly easy. For a field traveling along the z-axis a distance Δz, the phase can be approximately described as

$$\Phi(x, y, z) = e^{jk_0 n(x,y,z)\Delta z}. \tag{10}$$

The total phase accumulated in propagating from z_1 to z_2 depends on the index of the media along the path. Since the free space propagation step already includes a phase shift $e^{-jk_0\bar{n}\Delta z}$, the amount of phase shift due to the inhomogeneity is simply added to this

$$\Delta\Phi(x, y, z) = e^{jk_0(n(x,y,z)-\bar{n})\Delta z}. \tag{11}$$

The influence of the local index distribution on the propagation of the wave is included by multiplying the spatial wave, $\psi(x, y, \Delta z)$ by phase correction $\Delta\Phi(x, y, z)$ after each free space propagation step. This process is then repeated using $\Phi(x, y, z + \Delta z)$ as the source field for the next propagation step. The first step is to propagate the spatial mode a distance Δz. This requires using an FFT to determine the plane wave expansion, $\Phi(k_x)$, then advancing each plane wave a distance Δz and then reconverting the phase space superposition into a spatial field using an inverse FFT. Formally, using continuous variables to describe the step, the field at position $z + \Delta z$ is

$$\psi(x, y, \Delta z) = \frac{1}{2\pi}\int_{-\infty}^{\infty}\psi(k_x)e^{-j(k_x x + k_z \Delta z)}dk_x, \tag{12}$$

where k_z is the z-component of the k-vector for each ray. Each ray has a unique value of k_z, given by

$$k_z = \sqrt{\bar{n}k_0^2 - k_x^2}. \tag{13}$$

Evaluating the integral in eqn (12) using FFT is straightforward; however, the large magnitude of k_x makes the phase vary rapidly with Δz. Since the fast variation is of no interest to us, we usually separate it from the slow variation. This can be accomplished by writing k_z as

$$k_z = \bar{n}k_0 - \frac{k_x^2}{\bar{n}k_0 + \sqrt{\bar{n}^2 k_0^2 - k_x^2}}. \tag{14}$$

Note that this is a more exact version of eqn (13). In this form, the fast term ($\bar{n}k_0$) is distinct from the slow terms. The wave, after propagating a distance Δz in the homogeneous region, can then be expressed as

$$\psi(x, y, \Delta z) = \frac{e^{-j\bar{n}k_0\Delta z}}{2\pi}\int_{k_z > 0}\Phi(k_x)\exp\left[\frac{jk_x^2\Delta z}{\bar{n}k_0 + \sqrt{\bar{n}^2 k_0^2 - k_x^2}}\right]dk_x. \tag{15}$$

We changed the limits of integration to restrict the argument of the exponent to purely imaginary values, ensuring that no evanescent waves are included in the description of the wave propagation. Physically speaking, a complete description of a plane wave expansion requires evanescent waves, as they represent the loss mechanism to radiation modes. However, the lens step of the BPM technique assumes that the rays are travelling essentially parallel to z-axis. Evanescent waves are explicitly excluded from the expansion by restricting the possible values of k_z to real values only. Restricting the plane wave expansion to beams with large area and to waveguides which are weakly guiding helps insure that the k-vectors would be nearly parallel to the z-axis [11]. Finally, we add the contribution from the

lens by multiplying the propagated spatial field $\psi(x, y, \Delta z)$ by $\Phi(x, y, z)$. The process repeats by advancing the field forward by one more Δz. First, we describe a simple triangular profile waveguide. We choose an array size of 512 data points to describe the index profile, the spatial mode and the phase correction. A smaller array would be proportionally faster in calculation of speed, but we found that this size provided tolerable throughput speed. We arbitrarily choose an index profile 150 μm wide, with a guiding region of 10 μm wide. The step size in the calculation is 4 μm. The film and substrate index are 1.5 and 1.499, respectively. When an amplitude component moves off one side in the spatial FFT, it reappears on the other side of the spatial domain. This is in contrast to real waveguide, where we expect energy to continue travelling away from the core once it has been shed. There are several methods of apodizing. Signal processing algorithms often use triangular filters or hamming filters to proportionally attenuate the extreme spatial components. To reduce the reflections at analysis windows, we need some artificial boundary conditions. Since the simple transparent boundary condition (TBC) that is normally used in the FD (finite difference)–BPM cannot be used in FFT–BPM, some other artificial boundary conditions using complex refractive index materials or window functions have to be used to make the propagating fields decay properly near the edges of the analysis window. These artificial boundaries in FFT–BPM usually require skilled people to optimize the parameters to minimize reflections. BPM does not provide for energy loss due to radiation, so artificial means must be added to dissipate such modes. For BPM we require a flat transmission for the central portion of the waveguide but wish to add attenuation in the cladding region to simulate radiation mode losses and to prevent energy from wrapping around and re-entering the waveguide structure from the other side of the data array. The exact form of the apodizer is up to the user. In this paper, we choose to add a small attenuation to the cladding far from the region of the guided mode. The term 'aperture' defines the percentage of the aperture where the core and cladding are loss less. Here, we define the clear aperture to be 40% of the total aperture. The aperture must be larger than the final spatial extent of the guided mode to prevent adding unrealistic loss to the simulation. The magnitude of the attenuation is set through trial-and-error method. In the region of loss, each of step amplitude is attenuated by exp(–$atten$ Δz). Since in this simulation, $\Delta z = 4$ μm per step and $atten = 1500$ m^{-1}, the effective attenuation leads to a decrease of roughly 0.6% of the amplitude outside the aperture per step. This would add up to significant loss after hundreds of steps but does not act as a major perturbation to a field upon incident to the loss region. We found this value after trying several runs. Choosing the step length Δz depends on the guiding structure and wavelength. To stay within the region of validity for the BPM, Δz should satisfy [12],

$$\Delta z << 6k_0(k_e + k_w)^{-2}, \tag{16}$$

where k_e is the largest transverse component of the wave vector describing the guided electric field and k_w is the largest spatial frequency required to describe the index profile, if it were to be described as a Fourier superposition. To first order, the maximum spatial frequencies needed to describe both the electric field and the index profile can be approximated as,

$$k_e \approx \frac{2\pi}{x_0} \quad k_w \approx \frac{2\pi}{w}, \tag{17}$$

where x_0 is the characteristic half width of the mode and w, the half width of the waveguide. If we apply this criterion to the waveguide in this paper, where x_0 is approximately 10 μm for the eigenmode and w is approximately 5 μm, we find that $\Delta z < 12$ μm. Our choice of $\Delta z = 4$ μm satisfies this requirement. We used two examples to demonstrate the utility of BPM. First we used BPM to find the amplitude distribution in a graded index slab waveguide with triangular profile. Then we have simulated a mode propagating through a coupled waveguide. We set the trial mode characteristic width to 3 μm. We intentionally made the mode narrower than reasonably expected so the dynamics of the BPM process would be illustrated. Figure 5 shows a sample of the output as a function of the distance the simulated mode has travelled down the waveguide. The initial field distribution is a narrow Gaussian spike located at $z = 0$. This initial spatial mode can be described as a superposition of guided and radiation modes of this waveguide. As the initial amplitude propagates forward, the nonguided components begin to travel away from the guiding layer. The eigenmode becomes distinguished after travelling about one millimeter. The broad pedestal that the eigenmode sits on represents unguided energy that is radiating away from the waveguide. The unguided energy extends beyond the clear aperture and suffers attenuation with each step of calculation. Eventually the nonguided energy is totally dissipated. We can see the artifact of the calculation in the ripples that form on the pedestal for the plots between $z = 1$ and $z = 2$ mm. These ripples arise from interference between the outward-bound waves and those that have wrapped around from the other side that were not totally attenuated before reaching the boundary of the domains. After sufficient propagation, these interference features are damped out. The BPM successfully determines the shape of the mode for the triangular waveguide. The waveguide acts as a spatial filter to the input field distribution, eliminating all energy except that in the waveguides fundamental mode. We could substitute any reasonable index profile into the program and use the same technique to find the eigenmode.

5. Waveguide coupler

The beam propagation method is often used to evaluate the performance of either a coupled waveguide, a Y-junction or some other complex structure. We know that the field of a confined mode extends out beyond the core region. These evanescent tails can transfer energy from one waveguide to another if the dielectric structure is suitable. Here, we used BPM to 'experiment' with a coupled waveguide structure. We examined the propagation of a mode on a waveguide which is located adjacent to an identical guide. The index profile for this structure is plotted in Fig. 3(b). The coupler consists of two identical step-index waveguides with core thickness of 10 μm situated approximately 4 μm from each other. The evanescent field of either guide extends into the other guide. To begin the analysis, we launched a mode which is close to being an eigenmode of one of the individual waveguides. We found by simple trial and error that a Gaussian profile with an initial pulse width of 7 μm, gave an excellent approximation to the actual mode of the waveguide for a 1 μm wavelength light. We presented the result to launch the initial mode into the right-hand waveguide at $z = 0$. Figure 6 shows the evolution of the mode profile as it propagates down the waveguides. Each snapshot of the mode is taken after the field has propagated 1 mm down the waveguide. We see an evolution of the mode energy as it propagates along the coupled
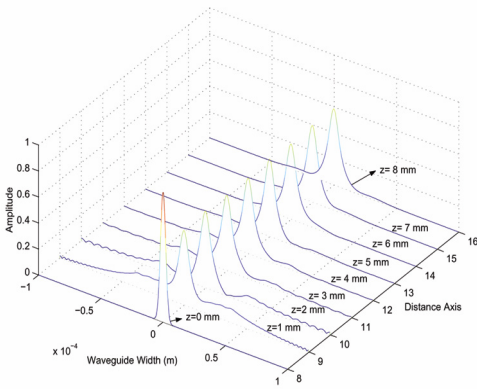
FIG. 5. Results of a BPM run on a triangular index slab waveguide. A trial mode with a Gaussian profile is launched at $z = 0$. As it travels down the guide, the unguided energy radiates away, while a guided mode emerges after some distance.
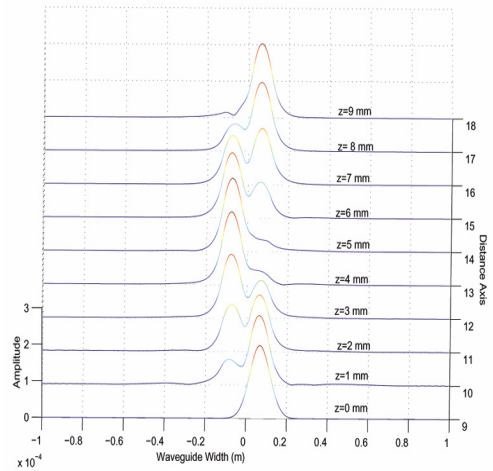

FIG. 6. The power in a coupled waveguide transfers back and forth as it propagates along the guide.

waveguide structure. After traveling approximately 4 mm down the waveguide, the energy has completely transferred over to the left-hand waveguide. As the beam continues to propagate, the energy transfers back to original guide. This process would continue indefinitely so long as the waveguides do not change their relative position or dimension. This is an extremely useful effect which can be exploited to make many practical devices such as couplers, taps, interferometers and wavelength-selective filters. For example, if the waveguides were brought together for only 1 mm, approximately 10% of the power from the first waveguide could be tapped, while the remaining 90% of the energy would continue along the main channel. The BPM method can be used to explore the effect of waveguide separation or mismatch on the coupling rate and efficiency. Figure 7 shows that the transfer rate of energy decreases as the waveguide separation is increased. The BPM technique provides an excellent way to evaluate the spatial structure of a mode as it propagates through a waveguide. But if the waveguide has sharp changes in index that could result in a reflection, BPM fails to account for the reflected wave or for possible interference effects between the forward and backward waves. Other techniques are needed to simulate such structures. We have emphasized that BPM does not provide for energy loss due to radiation. Hence it would not be applicable to multimode waveguide; of course, this method can easily be extended to 2D waveguide problem. Till now, we have examined the operation of a coupled waveguide using BPM. Now we use coupled mode theory to calculate the performance and compare theory with simulation. To review, the coupled slab waveguide structure is the same as shown in Fig. 3(b). We assumed that initially the mode energy is completely contained in the right-hand waveguide, but since this is a degenerate one there would be strong coupling.

Figure 8 shows how the power couples back and forth between the waveguides. By inspection, we see that the spatial coupling period is approximately 0.4 cm, which is exactly what we have observed in the BPM example. We have explored the theoretical basis for this behavior elsewhere [13].
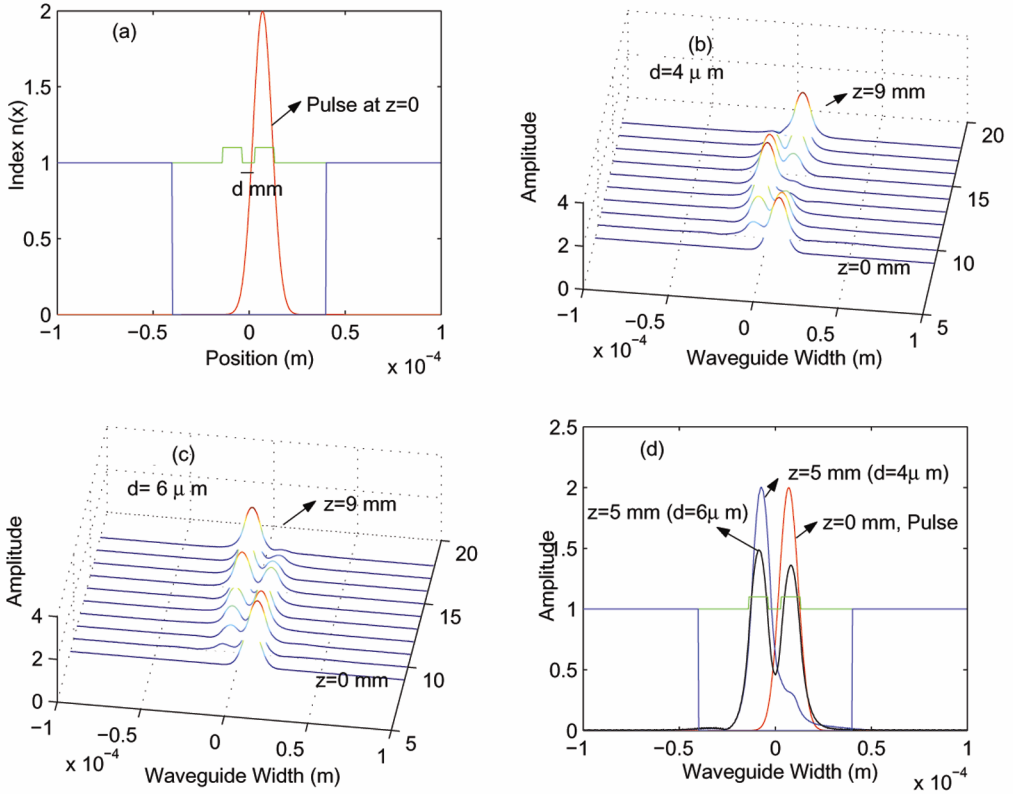
FIG. 7. (a) Index profile of two slab waveguides separated by only 4 μm while the initial amplitude profile is off-set to overlap the right-hand waveguide. (b) The power in a coupled waveguide during separation is 4 μm. (c) The power in a coupled waveguide during separation is 6 μm. (d) Comparison of the above two cases at simulation run length (z) of 5 mm.

6. Conclusion

We have used numeric techniques to evaluate difficult index profiles and to simulate the behavior of modes in a coupled waveguide. Using FFT, we have shown that a spatial wave can be described as a superposition of plane waves. With this, we can predict the wave propagation. We apply this knowledge to free space propagation and demonstrate how a wave with finite transverse dimension would diffract as it propagates. The local index of refraction will modify the cumulative phase of a propagating wave. By adding a phase correction to the spatial waveform, the combined effect of diffraction and guiding is described.

This work finds application in the following areas:

1. Our method successfully determines the shape of the mode for the triangular waveguide. One could substitute any reasonable index profile into our program and use the same technique to find the eigenmode.
2. The method can be used to evaluate the performance of a coupled waveguide, a Y-junction or some other complex structure. We know that the field of a confined mode
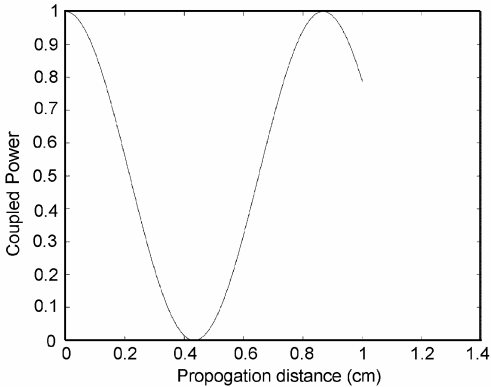
FIG. 8. The power in the original waveguide couples back an forth between the two waveguides. The coupling period for the power is approximately 0.4 cm.

extends out beyond the core region. These evanescent tails can transfer energy from one waveguide to another if the dielectric structure is suitable. We have explored the numerical technique for mode coupling and energy transfer between coupled waveguides in this paper. As an example, we have examined the propagation of a mode on a waveguide, which is located adjacent to an identical guide. We have also shown that the transfer rate of energy decreases as the waveguide separation is increased.

This paper will help the researchers to explore the effect of waveguide separation or mismatch on the coupling rate and efficiency.

References

1. J. Van Roey, J. Van der Donak, and P. E. Lagasse, Beam-propagation method: analysis and assessment, *J. Opt. Soc. Am.*, **71**, 803–810 (1981).

2. D. Yevick, and L. Thylen, Analysis of gratings by the beam-propagation method, *J. Opt. Soc. Am.*, **72**, 1084–1089 (1982).

3. R. Baets, and P. E. Lagasse, Calculation of radiation loss in integrated-optic tapers and Y-junction, *Appl. Opt.*, **21**, 1972–1978 (1982).

4. Anthony A. Tovar, and W. Lee, Casperson, Beam propagation in parabolically tapered graded-index waveguides, *Appl. Opt.*, **33**, 7733–7739 (1994).

5. M. D. Feit, and J. A. Freck, Jr, Light propagation in graded-index optical fibers, *Appl. Opt.*, **17**, 3990–3998 (1978).

6. L. Thylen, The beam propagation method: An analysis of its applicability, *Opt. Quantum Electron.*, **15**, 433–439 (1983).

7. J. Yamauchi, J. Shibayama, and H. Nakano, Beam propagation method using Padè approximant operators, *Trans. IEICE Jap.*, **J77-C-I**, 490–494 (1994).

8. Y. Chung, and N. Dagli, Assessment of finite difference beam propagation, *IEEE J. Quantum Electron.*, **26**, 1335–1339 (1990).

9. William Press, Brian P. Flannery, Saul A. Teukolsky, and William T. Vetterling, *Numerical methods*, Ch. 12, Cambridge University Press (1986).

10. B. Buckman, *Guided wave optics*, Saunders College (1992).

11. D. Marcuse, *Theory of dielectric waveguides*, 2nd edn, Academic Press (1991).

12. Lars Thylen, The beam propagation method: An analysis of its applicability, *Opt. Quantum Electron.*, **15**, 433–439 (1983).

13. Sanjeev Kumar Raghuwanshi, and T. Srinivas, Degenerate/non-degenerate modes coupling in an optical waveguide, Submitted to *XXXII Optical Society of India (OSI) Symp. on Contemporary Optics and Applications*, Baroda, India, March 1–3, 2007.

Nomenclature

BPM   =   Beam propagation method
FFT   =   Fast Fourier transform
DFT   =   Discrete Fourier transform
FD-BPM =   Finite difference beam propagation method
TBC   =   Transparent boundary condition